JACS
JOURNAL OF THE AMERICAN CHEMICAL SOCIETY
pubs.acs.org/JACS
Article

Formation of Graphene on Gold−Nickel Surface Alloys

Jeongjin Kim, Santosh K. Singh, Qing Liu, Christopher C. Leon, and S. T. Ceyer*

Cite This: J. Am. Chem. Soc. 2023, 145, 6299−6309
Read Online
ACCESS | Metrics & More | Article Recommendations

ABSTRACT: Nickel (Ni)-catalyzed growth of a single- or rotated-graphene layer is a well-established process above 800 K. In this report, a Au-catalyzed, low-temperature, and facile route at 500 K for graphene formation is described. The substantially lower temperature is enabled by the presence of a surface alloy of Au atoms embedded within Ni(111), which catalyzes the outward segregation of carbon atoms buried in the Ni bulk at temperatures as low as 400−450 K. The resulting surface-bound carbon in turn coalesces into graphene above 450−500 K. Control experiments on a Ni(111) surface show no evidence of carbon segregation or graphene formation at these temperatures. Graphene is identified by its out-of-plane optical phonon mode at 750 cm^{-1} and its longitudinal/transverse optical phonon modes at 1470 cm^{-1} while surface carbon is identified by its C−Ni stretch mode at 540 cm^{-1}, as probed by high-resolution electron energy-loss spectroscopy. Dispersion measurements of the phonon modes confirm the presence of graphene. Graphene formation is observed to be maximum at 0.4 ML Au coverage. The results of these systematic molecular-level investigations open the door to graphene synthesis at the low temperatures required for integration with complementary metal-oxide-semiconductor processes.

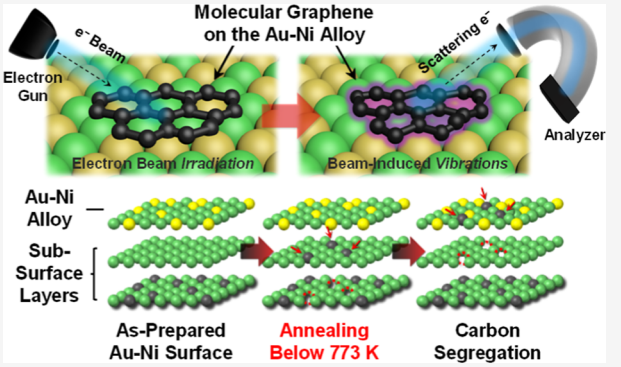

Downloaded via MASSACHUSETTS INST OF TECHNOLOGY on June 18, 2023 at 20:14:59 (UTC).
See https://pubs.acs.org/sharingguidelines for options on how to legitimately share published articles.

INTRODUCTION

Graphene, an emerging two-dimensional carbon material with faster electron mobility than silicon, higher electrical conductivity than copper, and greater hardness than steel, has been considered a new horizon for next-generation nanotechnology.[1,2] In particular, nanometer-scale fabrication of graphene layers with "magic" angle-rotated architectures[3,4] and size-controlled graphene nanoribbons[5,6] open up the possibility of field-effect transistor-based, flexible nanodevices.[7,8]

Metallic nickel (Ni) is well-established as a substrate to synthesize functional graphene layers via chemical vapor deposition (CVD) that involves its exposure at 1173−1273 K to a hydrocarbon (typically CH_4 or C_2H_2) and H_2 gas mixture.[9,10] The adsorbed hydrocarbon fragments produced by Ni-catalyzed dissociation of these hydrocarbons ultimately yield seeds of carbon rings that grow into epitaxial graphene layers.[11,12] In addition, given the relatively high solubility of carbon in Ni, much of the carbon resulting from the hydrocarbon dissociation dissolves in the Ni at the high temperatures at which graphene CVD is carried out, setting up an equilibrium distribution of dissolved and surface bound carbon, including adsorbed graphene.[13−15] Importantly, various investigations, including surface morphology imaging studies, clearly demonstrate that the growth rate of graphene as well as its quality are greatly influenced by the presence of subsurface carbon and its segregation to the surface.[16−19] These observations are supported by a variety of electronic structure calculations[20−22] and molecular dynamics simulations,[23,24] making it clear that the diffusion of dissociated carbon species in the near-surface region is critical in fabricating functional graphene on Ni substrates. Because the molecular mechanisms of hydrocarbon decomposition and of hydrocarbon fragment diffusion and segregation remain obscure, and because these processes affect the uniformity of carbon-ring networks, delicate and oftentimes arbitrary adjustments of the hydrocarbon to H_2 ratio, substrate temperature, and annealing rates are necessary to obtain the desired domain size and morphology of the graphene.[25,26]

To elucidate the mechanism of graphene formation on Ni, studies have been carried out where the growth of graphene is decoupled from the initial deposition of the hydrocarbon. In these cases, the Ni substrate is presaturated with carbon via a variety of methods,[27−32] and then, the growth of graphene is monitored in the absence of a hydrocarbon gas and as a function of substrate temperature. The graphene forms from the carbon that has segregated from the subsurface of the Ni

Received: December 11, 2022
Published: March 13, 2023

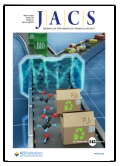

© 2023 American Chemical Society

https://doi.org/10.1021/jacs.2c13205
J. Am. Chem. Soc. 2023, 145, 6299−6309

substrate to its surface. The complex nature of carbon segregation from bulk Ni layers is illustrated in Figure 1.

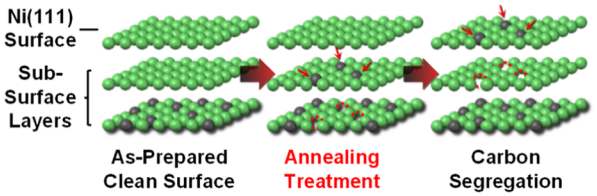

Figure 1. Schematic of subsurface carbon segregation by annealing the Ni(111) substrate.

Carbon atoms buried deep in the Ni lattice diffuse toward the near-surface by overcoming the thermal diffusion barrier in a Ni−C solution. Eventually, carbon atoms migrate from subsurface layers to the topmost layer, where carbon−carbon formation occurs and where the carbon clusters and carbon ring fragments ultimately coalesce into graphene. Involvement of a Ni_2C carbide phase in graphene growth as opposed to the addition of carbon atoms bound in three-fold hollow Ni sites to the growing carbon clusters and graphene network appears to depend on the specific experimental conditions of substrate temperature and of subsurface carbon concentration that are critical parameters dominating the intricate behavior of graphene growth.[33−36] With continued annealing, graphene grows at temperatures as low as 730 K.[34]

In this report, the effect of alloying Au atoms into the surface of Ni(111) on the evolution of graphene resulting from the segregation of carbon in the bulk Ni onto the surface is explored. It is found that the presence of a submonolayer of Au atoms randomly substituted for Ni atoms in a close-packed hexagonal lattice dramatically lowers the energy barrier for carbon segregation and graphene formation. Graphene is observed to be formed on Au−Ni(111) at temperatures as low as 450−500 K, coincident with the segregation of bulk carbon onto the surface. Neither carbon segregation to the surface nor graphene formation is observed on Ni(111) at this low temperature and conditions of extremely low carbon content in the Ni bulk.

The sole carbon source for both the Au−Ni(111) surface alloy and the Ni(111) surface experiments is the residual carbon in a single crystal of 99.999% pure Ni. Surface carbon is identified by its characteristic Ni−C stretch frequency, as probed with high-resolution electron energy-loss spectroscopy (HREELS). Graphene is similarly identified by the characteristic frequencies of the phonon modes of graphene adsorbed on Ni and by the dispersion of these modes.

Systematic HREELS measurements as a function of Au coverage ranging from 0.11 to 0.84 ML Au reveal that the amount of graphene formed is a maximum at 0.40 ML Au. This optimized morphology of the Au−Ni alloy at the topmost layer efficiently induces subsurface carbon diffusion from the bulk Ni to the surface where the resulting surface-bound carbon spontaneously assembles into metastable clusters which in turn coalesce into carbon-ring networks of graphene. These results report graphene synthesis on a Ni-based substrate at the lowest temperature currently known without plasma-enhanced decomposition of a carbon precursor[37] and open the door to graphene synthesis at the low temperatures compatible for integration with complementary metal-oxide-semiconductor (CMOS) processes.

EXPERIMENTAL SECTION

Procedure. A clean (111) surface morphology of a polished Ni single crystal, oriented to within 0.1° cut-accuracy, was prepared in an ultra-high-vacuum (UHV) chamber[38] (base pressure: 2×10^{-11} Torr) through multiple cycles of Ar^+ ion-bombardment sputtering (5×10^{-5} Torr Ar gas, 1.5 kV Ar^+ ion-incident energy) and subsequent substrate annealing at 1000 K for 20 min. This surface cleaning protocol was repeated until signals from common impurities (carbon, oxygen, and sulfur) were below the detection limit as measured by Auger electron spectroscopy using an incident energy of 2000 eV and employing a cylindrical mirror energy analyzer. The surface purity was also confirmed by the absence of energy-loss features in an HREEL spectrum employing a 127° cylindrical sector energy analyzer. The Ni(111) single crystal, whose temperature is variable at 77−1300 K, is attached to a multi-axis motion manipulator inside the analysis chamber, allowing its position to be optimized at the normal angle to the Auger spectrometer or 60° to the incident electron beam of the HREEL spectrometer. Each HREEL spectrum was recorded at the specular (θ = 60°) and an off-specular tilt angle of $2\Delta\theta$ degrees achieved by rotation of the Ni crystal by $\Delta\theta$ from the specular angle.[39] The full-width at half maximum (FWHM) of the elastically scattered electrons varied between 58 and 68 cm^{-1} using incident energies (E_i) ranging from 3.0 to 10.0 eV. Acquired spectra are normalized to the elastically scattered electron intensity of 10 kilocounts/s and are plotted against energy loss with a channel width of 8 cm^{-1}. Contour maps are created using a triangulation algorithm and a smoothening process on the normalized intensities as a function of energy loss. Intensities plotted in the contour maps between the tilt angles of $2\Delta\theta$ and the centers of the 8 cm^{-1} wide channels of energy loss at which spectra are measured were obtained by linear interpolation.

Preparation and Characterization of Au−Ni(111) Surface Alloys. After confirming the surface cleanliness of the Ni crystal (99.999%), less than 1 ML of Au atoms (99.999%) is vapor-deposited onto the Ni(111) substrate at 450 K at a rate of 0.01 ML/s, estimated by a quartz crystal microbalance. The Au-covered Ni(111) surface is immediately annealed at 773 K for 10 min to form a single layer of the Au−Ni surface alloy under UHV. Uniformity of the Au coverage across the surface is verified as previously described.[40] The absolute Au coverage is determined from the ratio of the Au (74 eV) Auger transition intensity measured in the derivative mode to that of Ni (64 eV), as shown in Figure 2. The derivative intensity of the Au transition increases proportionally with the amount of deposited Au atoms, whereas the Ni transition simultaneously attenuates owing to the Au−Ni alloy structure formation at the topmost layer. The intensities are corrected for the contribution from subsurface Ni atoms and relative cross-sections for excitation, as described elsewhere.[39,41] No loss features are observed in the HREEL spectra

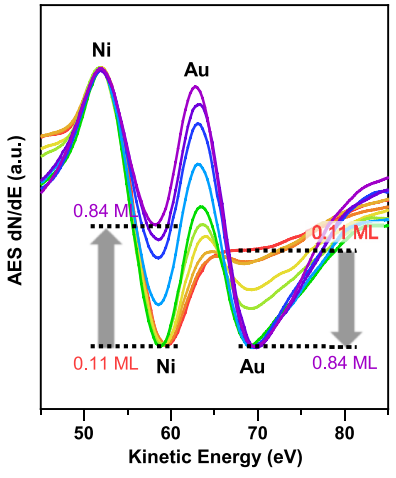

Figure 2. Derivative Auger electron spectra in region of Au and Ni transitions.

https://doi.org/10.1021/jacs.2c13205
J. Am. Chem. Soc. 2023, 145, 6299−6309

measured from this as-prepared alloy surface. This measure of surface cleanliness is particularly useful because the Au Auger transitions between 240 and 265 eV interfere with quantifying carbon.

Au−Ni Surface Alloy Structure in the Near-Surface Region. Each prepared Au−Ni surface maintains the hexagonally close-packed structure of a Ni(111) surface after replacement of Ni by Au atoms. However, because of significant lattice mismatch between the first and second layers due to the size difference between Ni and Au atoms, a structural transformation in the second layer occurs as the Au coverage approaches 0.3 ML. The phase transition involves a shift of the second layer Ni atoms from their fcc sites to hcp sites to relieve lattice strain, concomitantly forming triangular misfit dislocation loops[42] whose size depends on Au coverage[43] above 0.3 ML Au. This unique structural behavior of the Au−Ni surface alloy was previously established by atom-resolved imaging.[44]

RESULTS AND DISCUSSION

Identification of Graphene-like Vibrational Modes in the HREEL Spectra. Each clean and characterized Au−Ni alloy surface, prepared as described in the previous section, was flash annealed (ramp rate: 10 K/s) from 77 to 773 K, then quickly cooled to 77 K, at which temperature it was maintained for about 2−3 h. The alloy surface was again flash annealed to 773 K and quickly cooled to 77 K, at which temperature it was maintained for about 30 min, prior to obtaining the HREEL spectra at 77 K. The results are shown in Figure 3 as a function

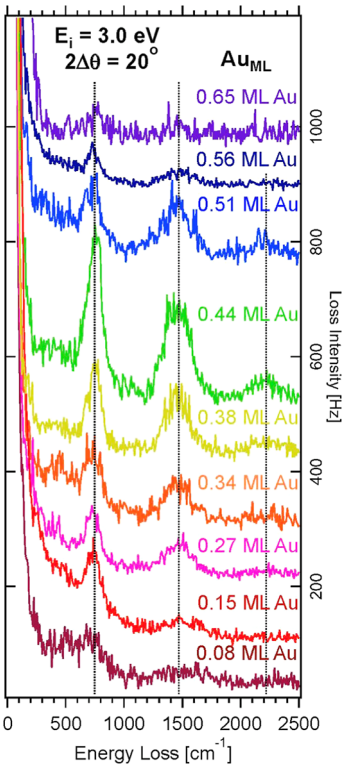

Figure 3. HREEL spectra at E_i = 3.0 eV and $2\Delta\theta = 20°$ as a function of Au coverage. Dotted gray lines are drawn at 750, 1470, and 2220 cm^{-1}.

of Au coverage. This annealing and cooling procedure was found to induce considerable segregation of subsurface carbon from the bulk Ni lattice and to maximize the intensities of the loss features. The spectra in Figure 3 are measured at an off-specular tilt angle ($2\Delta\theta = 20°$) and at E_i = 3.0 eV. No external hydrocarbon sources were introduced into the analysis chamber before or after the Ni substrate annealing/cooling treatments. The pressure in the analysis chamber is maintained below 1×10^{-10} Torr during all HREELS measurements.

The dominant features in Figure 3 are a pair of energy losses at 750 and 1470 cm^{-1}, which are most intense around 0.4 ML Au coverage. These vibrational frequencies are not characteristic of stretching or bending modes of common adsorbates on a metallic Ni surface, such as Au/Ni−O,[40] Au/Ni−CO,[41] Ni−S,[45] Ni−H_2O,[46] Ni−H,[47] or other hydrocarbon fragments.[48,49] Rather, these features are assigned to the out-of-plane optical (ZO) mode at 750 cm^{-1} and the in-plane longitudinal optical (LO) mode at 1470 cm^{-1} or the unresolved LO and in-plane transverse optical (TO) phonon modes at 1470 cm^{-1} of adsorbed graphene. The 1470 cm^{-1} mode is here designated as the LO/TO mode. These assignments are based on the correspondence of these frequencies with those previously measured, using HREELS, at or near the Γ point of the Brillouin zone, from a monolayer of graphene grown on Ni(111) via a CVD process.[50−52] In addition, a feature at about 2220 cm^{-1} becomes apparent in the HREEL spectra in Figure 3 around 0.34−0.5 ML Au coverage. This broad feature, whose intensity tracks the sum of the intensities of the ZO and LO/TO modes, is assigned to a combination band of ZO and LO/TO modes. Past HREEL spectra of a graphene monolayer on Ni(111)[50,51] do not extend to this higher energy loss regime, so no comparison is possible. The ZO and LO/TO mode features are also observable at the specular angle, but are much less intense, and thus are not plotted here. The weak intensity of these features at the specular angle, which indicates that these modes are not dipole active, is consistent with previously reported HREEL spectra.[50−52]

To confirm the assignment of these modes as those characteristic of graphene, their dispersion is probed through measurements of HREEL spectra as a function of the incident electron energy E_i and the tilt angle ($0° \leq 2\Delta\theta \leq 58°$), allowing the mode frequencies to be investigated as a function of parallel momentum transfer. Before acquiring HREELS signal from a 0.30 to 0.31 ML Au surface alloy at each primary electron energy of 3.0, 6.0, or 10.0 eV, the Au−Ni surface alloy is flash annealed to 773 K (ramp rate: 10 K/s) and then cooled quickly using liquid nitrogen and held at 77 K for 3 h. This flash anneal−cooling cycle is repeated three times, but in the last cycle, the alloy substrate is rapidly cooled to 293 K, the temperature at which the spectra are measured. Each spectrum, measured at incident energies of 3.0, 6.0, or 10.0 eV, is obtained every 6−10° over a tilt angle range of 0−58°, thereby providing a parallel momentum transfer $q_{\parallel}$ ranging from 0 to 0.8 $Å^{-1}$. As described in the previous section, the signal at each channel width is plotted as a function of frequency (or energy loss) at the mid-channel value and of the tilt angle to compose the intensity contour plots in Figure 4a−c. The intensities between the tilt angles at which the signal was acquired and in between the mid-channel frequencies are obtained by linear interpolation so that a continuous contour plot of intensities is obtained. In addition, the frequency at which the maximum intensity occurs is determined by a fit of a Lorentzian function to the elastic and loss features of each HREEL spectrum, and those maximum frequencies are plotted as a function of $q_{\parallel}$ in Figure 4d. The error bars (± 12 cm^{-1}) represent the standard error (1σ) of the mathematical fit result.

It is clear from the contour plots in Figure 4a−c that the intense HREELS signals appear at about 750 and 1470 cm^{-1}, corresponding to the ZO and LO/TO modes, and that the frequencies at which the highest intensities are observed do not

https://doi.org/10.1021/jacs.2c13205
J. Am. Chem. Soc. 2023, 145, 6299−6309

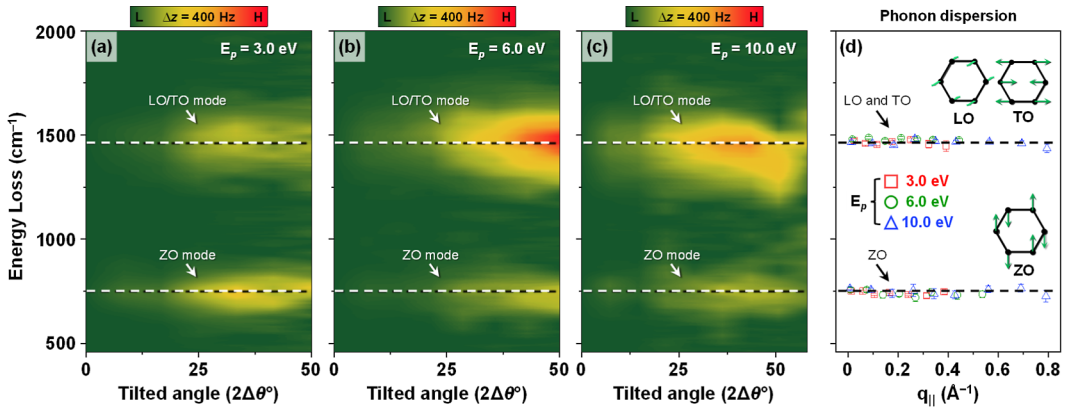

Figure 4. (a–c) Contours maps of HREEL intensities of out-of-plane (ZO) and in-plane (LO/TO) modes of graphene measured on a 0.30–0.31 ML Au–Ni surface alloy at 293 K after flash annealing treatments for E_i = 3.0 (a), 6.0 (b), and 10.0 (c) eV as a function of tilt angle ($2\Delta\theta°$). (d) Phonon dispersion relation for $0 \leq q_{||} < 0.8$ from measured HREEL spectra at E_i = 3.0 (red square), 6.0 (green circle), and 10.0 eV (blue triangle).

change significantly as the tilt angle increases. Correspondingly, a plot of the ZO and LO/TO mode frequencies versus parallel momentum transfer, $q_{||}$, in Figure 4d is also flat, indicating little dispersion over this range of $q_{||}$. Previous studies[53] of the dispersion relationship of single-layer graphene adsorbed on Ni(111) also show a lack of dispersion along both the Γ*M* and Γ*K* directions of the Brillouin zone for $q_{||}$ over the range $0 < q_{||} < 0.7$ Å^{-1}. For $0.7 < q_{||} < 0.8$ Å^{-1}, a slight decrease in the frequency of both the ZO and LO/TO modes has been observed previously for graphene on Ni(111),[50] and a similar decrease is observed in Figure 4c for the LO/TO mode at high tilt angle, corresponding to $q_{||}$ = 0.7–0.8 Å^{-1}. As shown in Figure 4d, a decrease in the frequency of both modes is also suggested at high values of $q_{||}$. It should be noted that the direction along the Brillouin zone over which the present dispersion measurements were made is not known, but that knowledge is inconsequential because the dispersion relationship is approximately symmetric around the Γ point for the ZO and LO modes. In contrast, the TO or transverse optical mode is only observable along the Γ*K* direction. However, its frequency is degenerate with the LO mode for low values of $q_{||}$ and then decreases by about 10% at $q_{||}$ = 0.8 Å^{-1}. The fact that neither decrease in frequency nor broadening of the 1470 cm^{-1} feature is apparent at high $q_{||}$ suggests that the present dispersion measurements are largely along the Γ*M* direction.

The absolute values of the experimental frequencies of the ZO and LO/TO modes of graphene adsorbed on Au–Ni(111) are slightly different from those measured on Ni(111), as expected for different substrates. Previously reported values for the ZO mode frequency for graphene on Ni(111), measured at or very near the Γ point,[50,51] range from 720 to 740 cm^{-1} and are slightly lower than the value of 750 cm^{-1} observed here. The weaker interaction between the metal 3d band of the alloy and the π orbitals of graphene likely shifts the ZO mode frequency to higher values, toward those of free-standing graphene at 860 cm^{-1}.[12,54] Indeed, intercalation of multiple layers of Au between a graphene layer grown on a Ni(111) substrate and the Ni(111) substrate resulted in a shift of the ZO mode to about 860 cm^{-1}.[52] The measured frequency of the LO(TO) mode, 1470 cm^{-1} at the Γ point of a graphene layer on Au–Ni(111), is also lower than that on Ni(111), 1500 cm^{-1}. The slightly lower frequency is attributed to a slightly longer C–C bond in graphene adsorbed on Au–Ni(111) because the epitaxial graphene layer is matched to a Ni lattice of Au–Ni that is slightly larger (and dependent on Au coverage[44]) than that of Ni(111), where the C–C distance is 2.49 Å. Similarly, the frequency of the LO(TO) mode in free-standing graphene is higher (1588 cm^{-1}) than that on Ni(111) because its graphene rings are not stretched to match the lattice constant of a substrate.[12]

Au Coverage Dependence of Graphene Formation on Au–Ni Surface Alloys. The extent of graphene formation is investigated as a function of Au coverage for Au–Ni surface alloys ranging from 0.08 to 0.65 ML Au coverage, as shown in Figure 3. In this set of spectra, evidence for graphene formation already appears at a Au coverage of 0.08 ML. As the Au coverage is increased to 0.15 ML Au and beyond, the intensities of the graphene features grow and reach a maximum at about 0.44 ML Au. Beyond 0.44 ML Au, the intensities decrease so much that at and beyond 0.65 ML Au, it is difficult to see the less intense LO/TO mode at 1470 cm^{-1}. Note that 0.79 ML Au amounts to 0.79 Au atom for every Ni atom and corresponds to complete Au coverage of the Ni(111) surface. It is noted that the spectra at 0.08, 0.34, and 0.44 ML Au coverage in Figure 3 are measured after exposure of the prepared alloy surface to H_2 or D_2 (for the purpose of studying graphene hydrogenation) and then flashing the crystal to 773 K to remove the hydrogen or deuterium prior to obtaining these spectra. However, the resulting spectra are indistinguishable from those spectra measured without H_2/D_2 exposure and its removal. In addition, another set of spectra as a function of Au coverage, not shown here, was also measured after a slightly different preparation (referred to as method II below), in which the prepared alloy surface was annealed at 500 K for 5 min, cooled to 80 K, held at 80 K for 30 min, and then annealed at 700 K for 5 min prior to measuring the spectrum. The salient features of this set of spectra, which includes a spectrum measured at 0.84 ML Au at which no graphene is observed, are identical to those shown in Figure 3 and validate the robustness of the graphene growth. The FWHM of the elastic feature is carefully maintained at the same value for each spectrum in each set in order to accurately quantify the integrated intensities of the graphene features as a function of Au coverage.

The intensities of the ZO (750 cm^{-1}) and LO/TO (1470 cm^{-1}) graphene loss features in Figure 3 (graphene preparation designated as method I) are integrated, along with those obtained from the alternate preparation of graphene

https://doi.org/10.1021/jacs.2c13205
J. Am. Chem. Soc. 2023, 145, 6299–6309

(described above and designated as method II), and these results are plotted in Figure 5a,b, respectively, as a function of

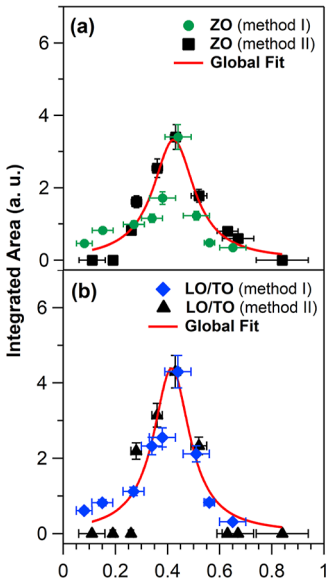

Figure 5. Plots of (a) ZO and (b) LO/TO integrated intensity vs Au coverage. Uncertainty in coverage, as described previously.[39−41] Error bars are $\pm\sigma$. Solid line is a global fit.

Au coverage. The values of the maximum intensity from each preparation method are normalized to each other because method I produces more graphene than method II, due to its higher annealing temperatures and longer waiting periods for graphene growth. The solid line is a global fit of a Lorentzian function to the integrated areas using a non-linear regression algorithm.[55] The intensities of both modes maximize at around 0.40 ML Au, indicating that this Au coverage optimizes the growth of graphene on this surface alloy.

Thermally Activated Subsurface Carbon Diffusion and Graphene Formation. With the identification of graphene phonon modes complete, the thermally activated growth of graphene is studied via in situ HREELS measurements on Au−Ni surface alloys as a function of the temperature at which the substrate is annealed. In particular, it is demonstrated that the alloying of Au atoms at less than 1 ML coverage with Ni(111) induces the segregation of dissolved carbon and its subsequent formation of graphene at the lowest temperatures known.

Figure 6a through 6d shows the HREELS spectra measured at 3.0 and 5.5 eV incident electron energy, and at an off-specular angle ($2\Delta\theta$ = 10°), as a function of annealing temperature for two Au coverages, 0.36 and 0.46 ML Au. Specifically, each alloy surface, prepared as described in the Experimental Section, is raised from 80 K to the indicated temperature with a ramp rate of 2 K/s and held at that annealing temperature for 5 min before being lowered to 80 K, the temperature at which each spectrum was measured. Spectra are shown for 50 K intervals over the annealing temperature range of 300−700 K.

Spectra measured from the 0.36 ML or 0.46 ML Au alloy surfaces that have been annealed to 300 or 350 K do not show any loss features. Only after annealing the surface to between 400 and 450 K does a broad feature (almost 100 cm^{-1} in width) centered at about 540 cm^{-1} begin to develop. It is attributed to a C−Ni stretch mode for a carbon atom bound in

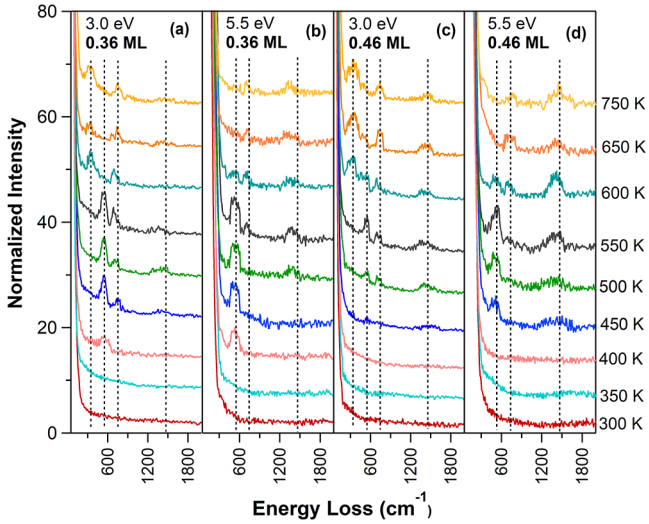

Figure 6. HREEL spectra of 0.36 ML Au−Ni(111) and 0.46 ML Au−Ni(111) alloy surfaces measured at an off-specular angle ($2\Delta\theta$ = 10°) at electron impact energies of (a,c) 3.0 eV and (b,d) 5.5 eV as a function of annealing temperature ranging from 300 to 700 K. Dotted lines indicate loss features at 340, 540, 750, and 1470 cm^{-1}.

a three-fold hollow Ni site, as assigned previously[56] and as supported by several calculated values of the frequency for this mode.[57−59] In some spectra in Figure 6, the appearance of the 540 cm^{-1} C−Ni stretch mode between 400 and 450 K is accompanied by the development of a feature centered around 700 cm^{-1}, which was assigned above to the out-of-plane ZO mode of graphene. Heating to 500−550 K results in increases in the intensity of the ZO mode and a slight blueshift of this mode as well as the discernible appearance of the less intense in-plane LO/TO mode of graphene at about 1400 cm^{-1}. The intensities of both modes increase with continued annealing to 600−700 K and the frequencies of both the out-of-plane ZO mode and the in-plane LO/TO mode shift up to their ultimate frequencies of 750 and 1470 cm^{-1}, respectively. The loss feature at about 540 cm^{-1} disappears upon heating to 600 K. In the case of spectra measured at 3.0 eV incident electron energy, a new feature centered around 340 cm^{-1} appears upon annealing to 600 K.

This set of spectra demonstrates the segregation of absorbed carbon to the surface and the aggregation of this carbon to form graphene as a function of the annealing temperature of the alloy. In particular, these spectra show that no carbon is present on the surface below an annealing temperature of 400 K. Once the alloy is annealed to between 400 and 450 K, thermal activation enables the dissolved carbon to emerge onto the surface, as evidenced by the C−Ni feature at 540 cm^{-1}. Simultaneously, the adsorbed carbon forms ring-like structures on the surface that presumably aggregate into a graphene-like structure. With additional annealing at higher temperatures, the intensities of the graphene modes continue to increase, indicating that the graphene structure continues to grow. In addition, the blueshift in the frequencies of the ZO and LO/TO modes with additional annealing signals that the size of the graphene network grows because the frequencies of the ring vibrations (500−666 cm^{-1}), such as the out-of-plane drumhead mode, of polycyclic aromatic hydrocarbons also blueshift with increasing hydrocarbon size.[60] The ultimate intensities of the graphene modes in the Figure 6 series of spectra are much less than those observed in Figure 3 and some of the

https://doi.org/10.1021/jacs.2c13205
J. Am. Chem. Soc. 2023, 145, 6299−6309

frequencies, particularly that of the LO/TO mode, are not at their ultimate high value. These differences reflect the smaller domain size of the graphene grown in Figure 6 than that in Figure 3. Figure 3 spectra were obtained after more cycles of significantly higher annealing temperature (773 K) and longer periods of cooling, allowing the graphene domain size to grow beyond that in Figure 6.

As the annealing temperature is increased, it is also clear, by the disappearance of the C−Ni stretch mode at 540 cm^{-1}, that the adsorbed carbon not incorporated into the graphene network dissolves into the bulk at around 600 K. This temperature of 600 K for adsorbed carbon dissolution on Au/Ni(111) is slightly lower than but still consistent with the temperatures of 675−700 K observed previously[61,62] for surface carbon dissolution into Ni(111). Interestingly, a new feature at 340 cm^{-1} appears simultaneously with the disappearance of the 540 cm^{-1} feature. However, the 340 cm^{-1} loss feature is apparent only in the spectra measured at 3.0 eV incident electron energy. This observation is significant because the 3.0 eV incident electrons have a significantly longer mean free path into the metal than the 5.5 eV electrons.[63] The longer mean free path enables excitation of vibrational modes of species buried beneath the surface.[64] Therefore, the loss feature at 340 cm^{-1} is tentatively assigned to the vibration of a carbon atom beneath the surface.

Temperature-dependent experiments that are not shown here were also carried out as a function of Au coverage, but no discernible effect of Au coverage over the range of 0.11−0.67 ML Au on the lowest temperature at which carbon segregates to the surface was observable.

The performance of the Au−Ni(111) surface alloy for graphene formation via segregation of bulk carbon to the surface is now compared to that of Ni(111). Figure 7 shows a set of spectra taken under similar conditions to Figure 6 after annealing Ni(111) to the temperatures shown over a range of 80−750 K. The spectra are measured at an off-specular angle ($2\Delta\theta = 20°$) and at E_i = 3.0 and 5.5 eV. It is clear that unlike the Au−Ni(111) surface alloy, no loss features corresponding to a C−Ni stretch or graphene ring modes are observed. Hence, neither carbon segregation to the surface nor graphene formation is observed on Ni(111) at this low temperature for this relatively low concentration of absorbed carbon. The present result is consistent with previous work where temperatures of 1400 K were required for graphene formation via segregation of carbon whose source was its naturally occurring abundance in Ni.[29]

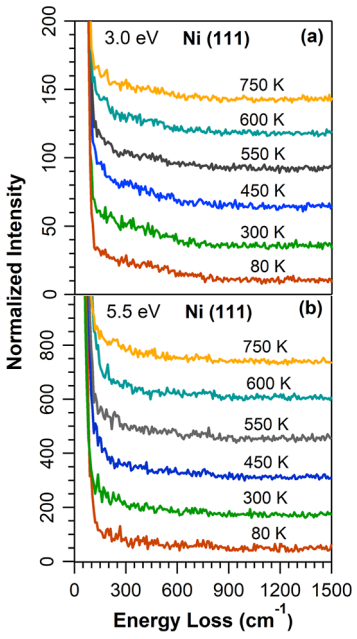

Figure 7. HREEL spectra of the Ni(111) surface measured at an off specular angle ($2\Delta\theta = 20°$) at E_i = (a) 3.0 and (b) 5.5 eV as a function of annealing temperature ranging from 80 to 750 K.

Clearly, this result demonstrates that the presence of a submonolayer of Au atoms randomly substituted for Ni atoms in a close hexagonally packed lattice greatly lowers the barrier for diffusion of the dissolved carbon onto the surface. In turn, the adsorbed carbon atoms, likely bound as sp^3−C−Ni species, spontaneously form carbon ring networks that ultimately aggregate into a graphene structure at temperatures as low as 500 K.

DISCUSSION

This section discusses possible mechanisms for the Au catalysis of carbon segregation and of graphene formation on a Au/Ni(111) surface alloy and the role of the size of Ni domains on a Au/Ni(111) surface alloy. It also compares the present result with those from a few studies where the structure and chemical composition of the catalyst resulting from the addition of Au to polycrystalline Ni or crystalline Ni is unknown.

Lower Barrier for Carbon Segregation on Au−Ni Surface Alloys. Setting aside the observation that Au catalyzes graphene formation, the above results clearly demonstrate that the presence of a submonolayer of Au randomly substituted for Ni in a close hexagonally packed lattice greatly lowers the barrier for diffusion of the dissolved carbon onto the surface, as evidenced by the appearance of the 540 cm^{-1} C−Ni stretch mode at about 400−450 K. The lower barrier is a consequence of changes in the geometry and electronic structure at the surface and near-surface of the alloy as compared to Ni(111). While these effects are strictly inextricable, their thoughtful separation enables physical insights into the origin of the lower barrier on a Au−Ni surface alloy. For example, incorporation of Au atoms into the Ni lattice results in a larger average lattice constant meaning that the center-to-center spacing of Ni atoms on the alloy is slightly larger[44] compared to that on Ni(111) (2.489 Å) and is dependent on Au coverage. The average lattice spacing has been determined from scanning tunneling microscopy (STM) measurements to be well described by the average of the lattice constant of a pure Au layer and that of a pure Ni layer. The less densely packed configuration of the Au−Ni alloy surface compared to a Ni(111) surface is likely a major contributor to the lowering of the barrier for emergence of an absorbed carbon atom from the layer just beneath the surface to the top of the surface atoms.

In addition, for Au coverages above 0.3 ML, a reconstruction of the second layer, which is composed entirely of Ni atoms, is present. It is characterized by missing rows of Ni atoms where each missing row makes a 60° angle to another missing row, creating a triangular configuration of missing rows known as a triangular dislocation loop.[44] These loops form to reduce the strain between the surface layer, whose lattice constant is larger than that of the second layer due to the presence of Au, and the second layer composed entirely of Ni atoms. The loops allow the atoms in the surface layer to move into more highly

https://doi.org/10.1021/jacs.2c13205
J. Am. Chem. Soc. 2023, 145, 6299−6309

coordinated positions with the second layer Ni atoms, thereby reducing the overall potential energy of the system. Of note is that the surface atoms immediately above the dislocation loops, whether they be Ni or Au atoms, are slightly "sunken" below the surface plane because the second layer atoms are missing from these positions. This geometric configuration suggests that the barrier for movement of a carbon atom bound in a dislocation loop to the surface is significantly lower than that for a subsurface carbon atom just below a Ni(111) surface and hence an additional underlying reason for carbon surface segregation at lower temperatures on a Au−Ni surface alloy than that on Ni(111).

Another contribution to the lowering of the barrier to surface segregation of carbon derives from the change in the stacking arrangement of the top five layers due to the reconstruction. In the regions of the dislocation loops, the stacking of the top five layers is changed from the canonical pattern of ABCAB stacking (where A represents the top layer) of a fcc crystal to BACAB stacking. This change arises from the shift of the second layer Ni atoms from their fcc sites to hcp sites once a chain of second layer Ni atoms is ejected, as described previously.[40] The result of this shift aligns the three-fold hollow sites of each layer, or more accurately, the octahedral interstitial sites, from the fifth layer to effectively the top layer, creating a low-barrier tunnel for the carbon atoms to move from the fifth layer to the surface.

Electronic effects also play a role in the magnitude of the barrier. The 3d band center of the Au−Ni alloy is lower in energy than it is for Ni(111) and smoothly decreases to that more closely matching Au as the Au coverage increases, with concomitant widening of the d band.[65−68] Consequently, overlap of the 3d band of the alloy with orbitals of carbon atoms is less energetically favorable, and therefore, adsorbates are generally less strongly bound on the Au−Ni(111) surface alloy. The binding energy difference between a carbon atom adsorbed on a three-fold hollow site of Ni(111) and one adsorbed on a three-fold hollow site consisting of two Ni atoms and a Au atom has been calculated to be 45 kcal/mol.[69] Even in the unlikely scenario where the absolute barrier height is unaffected by an electronic structure change, the fact that the adsorbate is significantly less strongly bound will result in a lower effective barrier.

Graphene Formation on Au−Ni Surface Alloys and Au Dependence. Once carbon atoms, likely bound as sp^3−C−Ni species, emerge onto the surface at the relatively low temperatures of 400−450 K, they spontaneously form carbon ring networks that ultimately aggregate into a graphene structure at temperatures as low as 500 K. This observation indicates that if a barrier to carbon ring formation exists, its magnitude is comparable to or less than that for surface segregation and hence is surmountable at temperatures between 450 and 500 K. Indeed, a density functional calculation on Ni suggests such is the case where the barrier for surface segregation is found to be 1.4 eV while that for addition of a carbon atom to a carbon ring network is calculated as 0.9 eV.[70]

Because carbon atoms are more stable in their interaction with Ni than that with Au,[69] it is likely that the carbon atoms accumulate in the Ni-rich islands of the surface and in the subsurface just below the Ni-rich islands. Quantum mechanical molecular dynamics simulations on Ni(111) have shown that the kinetics of large domain graphene formation is favorable at high carbon concentrations.[71,72] This carbon accumulation within the randomly sized Ni patches or islands of the alloy surface surrounded by the randomly distributed Au atoms may enhance graphene formation. It is also very likely that the dislocation loops facilitate the accumulation of subsurface carbon just below the surface because those loops constitute missing rows of Ni atoms in a triangular pattern. In turn, the surface above those loops, particularly if the surface atoms are part of the Ni islands, is likely covered with high coverages of carbon atoms that efficiently form bonds, ultimately leading to graphene. It is not known whether carbon−carbon bond formation occurs only between carbon adsorbed on Ni atoms or whether some bonds form between carbon atoms that are adjacent to Au atoms. Again, because carbon is bound much less strongly in the vicinity of Au, the barrier to carbon−carbon bond formation may be lower for those carbon atoms as compared to those solely bound to Ni atoms present at some distance from Au atoms. This statement is supported by the observation that the lowest temperature at which carbon has been observed to add to a graphene network on Ni(111) is about 700 K,[18] which is a considerably higher temperature than that observed here on Au−Ni(111).

The optimal Au coverage for graphene formation is found to be about 0.4 ML Au, a value that is the result of a multitude of competing factors and is best illustrated by Figure 8 that shows

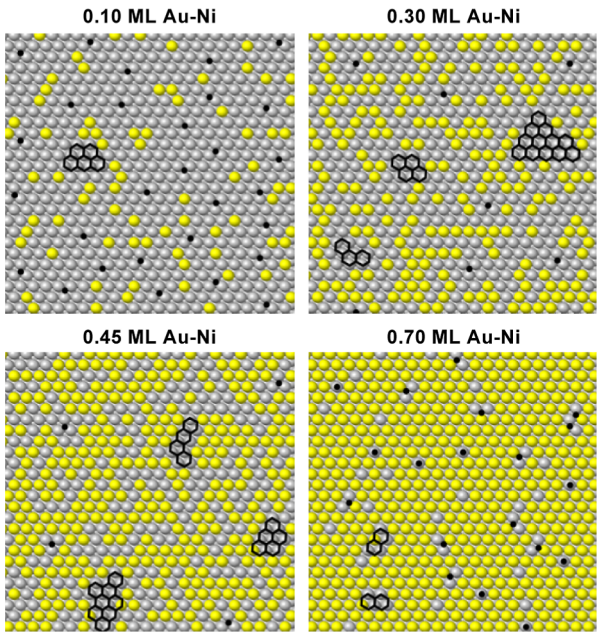

Figure 8. Simulated Au−Ni(111) surface alloys at selected Au coverages from 0.10 to 0.70 ML. Gray balls are Ni atoms, yellow balls are Au atoms, black dots are isolated C atoms, and hexagonal structures are graphene rings.

an idealized surface structure of the Au−Ni(111) alloy at 0.10, 0.30, 0.45, and 0.70 ML Au. The Ni atoms of this simulated closed packed structure, shown as gray balls, have been replaced randomly by Au atoms, shown as yellow balls. The small black dots and the hexagonal structures represent isolated C atoms and graphene rings, respectively. The simulated C coverage is set at 0.10 ML, where 1 ML is equivalent to the packing density of a monolayer of Ni atoms on a Ni(111) surface, for the 0.10, 0.30, and 0.45 ML Au surfaces. The C coverage is less than 0.10 ML at 0.70 ML Au, as shown in Figure 8.

https://doi.org/10.1021/jacs.2c13205
J. Am. Chem. Soc. 2023, 145, 6299−6309

At 0.10 ML Au coverage, while it is possible for tiny graphene flakes to be formed, the majority of the carbon exists as isolated atoms that are randomly distributed on three-fold hollow Ni sites, as evidenced by our observation of faint suggestions of graphene vibrational modes. At this low Au coverage, the average lattice constant remains very close to the value of Ni(111), and therefore, the barrier to surface segregation is not sufficiently lowered to result in a sufficient amount of surface carbon to form graphene effectively. In addition, if dissolved carbon only emerges at sites between Au and Ni atoms and where the barrier is therefore low, the Au concentration may simply not be high enough to effect a sufficient coverage of surface carbon. The resulting long distances between isolated carbon atoms may hinder the growth of graphene seeds.

As the Au coverage increases to 0.30 and 0.45 ML, the effective lattice constant becomes larger and the number of Au atoms that electronically perturbs the Ni electronic structure is larger, making the surface segregation barrier lower and thereby increasing the carbon coverage. In addition, triangular dislocation loops in the second layer are present at 0.30 ML Au and higher Au coverages and may serve as a reservoir for dissolved carbon, ultimately enhancing the surface carbon coverage. Even if the carbon coverage does not change from that at 0.1 ML Au, as shown in Figure 8, it is clear that the surface area of the Ni islands is reduced. Hence, the effective carbon coverage increases, likely facilitating the growth of the graphene network, as shown by dynamics simulations discussed above.[71,72] Assuming that graphene grows only on the Ni islands and is constrained to remain within the boundaries of the Ni islands, Figure 8 shows that the Ni islands can accommodate graphene flakes with 10 or more rings at coverages between 0.3 and 0.45 ML Au. However, given that Au is known to intercalate[52] between a graphene layer adsorbed on Ni and the Ni substrate, it seems possible and likely that as the graphene grows, the carbon-ring networks can extend over the Au atoms and Au islands, leading to the lifting of the growing graphene layer over Au. This behavior would lead to the formation of a graphene network larger than the area of the Ni islands. Indeed, quasi-free-standing graphite on Ni(111) has been produced by Au intercalation.[54] It is also interesting to consider whether the presence of Au atoms at these coverages stabilizes the growing graphene by making the reverse reaction, carbon−carbon bond cleavage of the carbon−carbon bonds within the graphene rings, less favorable. Previous simulations show that the dissociation of carbon−carbon triple bonds on a Au−Ni alloy becomes less energetically favorable as the Au content is increased.[73]

As the Au coverage increases beyond 0.5 ML and the alloy surface becomes more Au-like, the intensities of the graphene phonon modes decrease, meaning that the size and amount of graphene formation decrease, until no graphene is formed close to a full layer of surface Au, at 0.79 ML Au. As shown in Figure 8, islands of two or more Ni atoms at 0.7 ML Au are sparse and hence do not provide Ni areas large enough for graphene rings to grow or aggregate.

Previous Studies of Graphene Formation on Ni Substrates Doped with Au. Two studies of graphene formation via CVD of CH_4/H_2 or C_2H_2/H_2 as the carbon source have previously been carried out on Ni substrates doped with Au.[74,75] Both previous studies note a relatively low temperature of 730 K at which graphene is formed upon addition of Au to the Ni substrate but not the low temperature of 450−500 K that is observed here. Unlike the present work, the formation of a stable Au−Ni alloy is neither verified nor are the surface elemental compositions and structures known. It is likely that a well-formed Au−Ni surface alloy is required for maximum catalytic effect. However, the graphene produced on the Ni substrate with added Au in these previous studies is of higher quality and of larger area than that synthesized on Ni alone. It is suggested that the Au atoms occupy step edge sites that block the growth of multiple layers of graphene. The blocked step edges allow the graphene to grow uninterrupted from one facet to another and prevent graphene from forming multiple layers, a model supported by density functional calculations.[76,77] An additional electronic structure investigation also suggests that Au atoms stabilize the edges of the growing graphene from dissociation,[78] as discussed above.

SUMMARY AND CONCLUSIONS

The addition of submonolayers of Au to a Ni(111) crystal results in the formation of a surface alloy that is shown to catalyze the segregation of dissolved carbon onto the surface at substrate temperatures as low as 400−450 K and to catalyze the synthesis of graphene at substrate temperatures as low as 450−500 K. These temperatures are the lowest ones recorded for these processes on a Ni single crystal. Neither carbon segregation nor graphene formation is observed to occur on Ni(111) between 80 and 750 K under these conditions of low intrinsic carbon concentrations in the Ni crystal bulk. Clearly, the small amounts of Au alloyed into the Ni surface have a dramatic effect on the barrier for bulk to surface diffusion and to graphene formation. The segregation barrier is significantly lowered as a result of a slightly larger lattice constant of the alloy surface as well as a reconstruction in the second layer of Ni atoms that provide a lower energy pathway for the carbon atoms to make their way onto the surface. Electronic effects of the Au atoms result in less strong binding of the carbon atoms in the near vicinity of Au and in turn lower the barrier to both surface segregation in the vicinity of a Au atom and to addition of a carbon atom or a carbon cluster onto a growing graphene network. In addition, the kinetics of graphene growth is likely accelerated due to carbon accumulation in the dislocation loops of the second layer and the higher effective carbon coverage within the Ni islands of the Au−Ni(111) surface alloy. Finally, the presence of Au stabilizes the growing graphene network from the reverse reaction, its dissociation, by increasing the barrier for carbon−carbon bond cleavage. Graphene formation on Au−Ni(111) is observed to be a maximum at about 0.4 ML Au coverage, where the elementary steps for its formation and the morphological structure of the alloy surface are optimized. These results introduce the possibility of graphene synthesis at the low temperatures required for integration with CMOS processes.

AUTHOR INFORMATION

Corresponding Author

S. T. Ceyer − *Department of Chemistry, Massachusetts Institute of Technology, Cambridge, Massachusetts 02139, United States;* orcid.org/0000-0002-9989-6622; Email: stceyer@mit.edu

Authors

Jeongjin Kim − *Department of Chemistry, Massachusetts Institute of Technology, Cambridge, Massachusetts 02139, United States;* orcid.org/0000-0002-3790-1684

https://doi.org/10.1021/jacs.2c13205
J. Am. Chem. Soc. 2023, 145, 6299−6309

Santosh K. Singh − *Department of Chemistry, Massachusetts Institute of Technology, Cambridge, Massachusetts 02139, United States*

Qing Liu − *Department of Chemistry, Massachusetts Institute of Technology, Cambridge, Massachusetts 02139, United States*

Christopher C. Leon − *Department of Chemistry, Massachusetts Institute of Technology, Cambridge, Massachusetts 02139, United States*

Complete contact information is available at: https://pubs.acs.org/10.1021/jacs.2c13205

Notes

The authors declare no competing financial interest.

■ ACKNOWLEDGMENTS

This research was partially supported by Eni S.p.A. through the MIT Energy Initiative and by the National Science Foundation CHE-1900109.

■ REFERENCES

(1) Geim, A. K. Graphene: Status and Prospects. *Science* **2009**, *324*, 1530−1534.

(2) Bonaccorso, F.; Colombo, L.; Yu, G.; Stoller, M.; Tozzini, V.; Ferrari, A. C.; Ruoff, R. S.; Pellegrini, V. Graphene, Related Two-Dimensional Crystals, and Hybrid Systems for Energy Conversion and Storage. *Science* **2015**, *347*, 1246501.

(3) Cao, Y.; Fatemi, V.; Fang, S.; Watanabe, K.; Taniguchi, T.; Kaxiras, E.; Jarillo-Herrero, P. Unconventional Superconductivity in Magic-Angle Graphene Superlattices. *Nature* **2018**, *556*, 43−50.

(4) Yoo, H.; Engelke, R.; Carr, S.; Fang, S.; Zhang, K.; Cazeaux, P.; Sung, S. H.; Hovden, R.; Tsen, A. W.; Taniguchi, T.; Watanabe, K.; Yi, G.-C.; Kim, M.; Luskin, M.; Tadmor, E. B.; Kaxiras, E.; Kim, P. Atomic and Electronic Reconstruction at the van der Waals Interface in Twisted Bilayer Graphene. *Nat. Mater.* **2019**, *18*, 448−453.

(5) Han, M. Y.; Özyilmaz, B.; Zhang, Y.; Kim, P. Energy Band-Gap Engineering of Graphene Nanoribbons. *Phys. Rev. Lett.* **2007**, *98*, 206805.

(6) Wang, X.; Ouyang, Y.; Li, X.; Wang, H.; Guo, J.; Dai, H. Room-Temperature All-Semiconducting Sub-10-nm Graphene Nanoribbon Field-Effect Transistors. *Phys. Rev. Lett.* **2008**, *100*, 206803.

(7) Britnell, L.; Gorbachev, R. V.; Jalil, R.; Belle, B. D.; Schedin, F.; Mishchenko, A.; Georgiou, T.; Katsnelson, M. I.; Eaves, L.; Morozov, S. V.; Peres, N. M. R.; Leist, J.; Geim, A. K.; Novoselov, K. S.; Ponomarenko, L. A. Field-Effect Tunneling Transistor Based on Vertical Graphene Heterostructures. *Science* **2012**, *335*, 947−950.

(8) Jang, H.; Park, Y. J.; Chen, X.; Das, T.; Kim, M.-S.; Ahn, J.-H. Graphene-Based Flexible and Stretchable Electronics. *Adv. Mater.* **2016**, *28*, 4184−4202.

(9) Mafra, D. L.; Olmos-Asar, J. A.; Negreiros, F. R.; Reina, A.; Kim, K. K.; Dresselhaus, M. S.; Komh, J.; Mankey, G. J.; Araujo, P. T. Ambient Presure CVD of Graphene on Low Index Ni Surfaces using Methane: A Combined Experimental and First Principles Study. *Phys. Rev. Mater.* **2018**, *2*, 073404.

(10) Chae, S. J.; Güneş, F.; Kim, K. K.; Kim, E. S.; Han, G. H.; Kim, S. M.; Shin, H.-J.; Yoon, S.-M.; Choi, J.-Y.; Park, M. H.; Yang, C. W.; Pribat, D.; Lee, Y. H. Synthesis of Large-Area Graphene Layers on Poly-Nickel Substrate by Chemical Vapor Deposition: Wrinkle Formation. *Adv. Mater.* **2009**, *21*, 2328−2333.

(11) Losurdo, M.; Giangregorio, M. M.; Capezzuto, P.; Bruno, G. Graphene CVD Growth on Copper and Nickel: Role of Hydrogen in Kinetics and Structure. *Phys. Chem. Chem. Phys.* **2011**, *13*, 20836−20843.

(12) Dahal, A.; Batzill, M. Graphene−Nickel Interfaces: A Review. *Nanoscale* **2014**, *6*, 2548−2562.

(13) Shelton, J. C.; Patil, H. R.; Blakely, J. M. Equilibrium Segregation of Carbon to a Nickel (111) Surface: A Surface Phase Transition. *Surf. Sci.* **1974**, *43*, 493−520.

(14) Blakely, J. M. Segregation to Surfaces: Dilute Alloys of the Transition Metals. *Crit. Rev. Solid State Mater. Sci.* **1978**, *7*, 333−355.

(15) Eizenberg, M.; Blakely, J. M. Carbon Monolayer Phase Condensation on Ni(111). *Surf. Sci.* **1979**, *82*, 228−236.

(16) Li, X.; Cai, W.; Colombo, L.; Ruoff, R. S. Evolution of Graphene Growth on Ni and Cu by Carbon Isotope Labeling. *Nano Lett.* **2009**, *9*, 4268−4272.

(17) Weatherup, R. S.; Amara, H.; Blume, R.; Dlubak, B.; Bayer, B. C.; Diarra, M.; Bahri, M.; Cabrero-Vilatela, A.; Caneva, S.; Kidambi, P. R.; Martin, M.-B.; Deranlot, C.; Seneor, P.; Schloegl, R.; Ducastelle, F.; Bichara, C.; Hofmann, S. Interdependency of Subsurface Carbon Distribution and Graphene−Catalyst Interaction. *J. Am. Chem. Soc.* **2014**, *136*, 13698−13708.

(18) Patera, L. L.; Africh, C.; Weatherup, R. S.; Blume, R.; Bhardwaj, S.; Castellarin-Cudia, C.; Knop-Gericke, A.; Schloegl, R.; Comelli, G.; Hofmann, S.; Cepek, C. In Situ Observations of the Atomistic Mechanisms of Ni Catalyzed Low Temperature Graphene Growth. *ACS Nano* **2013**, *7*, 7901−7912.

(19) Patera, L. L.; Bianchini, F.; Africh, C.; Dri, C.; Soldano, G.; Mariscal, M. M.; Peressi, M.; Comelli, G. Real-Time Imaging of Adatom-Promoted Graphene Growth on Nickel. *Science* **2018**, *359*, 1243−1246.

(20) Zhu, Y.-A.; Dai, Y.-C.; Chen, D.; Yuan, W.-K. First-Principles Study of C Chemisorption and Diffusion on the Surface and in the Subsurfaces of Ni(111) During the Growth of Carbon Nanofibers. *Surf. Sci.* **2007**, *601*, 1319−1325.

(21) Wang, S.-G.; Liao, X.-Y.; Cao, D.-B.; Li, Y.-W.; Wang, J.; Jiao, H. Formation of Carbon Species on Ni(111): Structure and Stability. *J. Phys. Chem. C* **2007**, *111*, 10894−10903.

(22) Xu, J.; Saeys, M. First Principles Study of the Stability and the Formation Kinetics of Subsurfaces and Bulk Carbon on a Ni Catalyst. *J. Phys. Chem. C* **2008**, *112*, 9679−9685.

(23) Li, H. B.; Page, A. J.; Wang, Y.; Irle, S.; Morokuma, K. Subsurface Nucleation of Graphene Precursors near a Ni(111) Step Edge. *Chem. Commun.* **2012**, *48*, 7937−7939.

(24) Jiao, M.; Song, W.; Qian, H.-J.; Wang, Y.; Wu, Z.; Irle, S.; Morokuma, K. QM/MD Studies on Graphene Growth from Small Islands on the Ni(111) Surface. *Nanoscale* **2016**, *8*, 3067−3074.

(25) Shu, H.; Tao, X.-M.; Ding, F. What are the Active Carbon Species during Graphene Chemical Vapor Deposition Growth? *Nanoscale* **2015**, *7*, 1627−1634.

(26) Zhang, Y.; Zhang, L.; Zhou, C. Review of Chemical Vapor Deposition of Graphene and Related Applications. *Acc. Chem. Res.* **2013**, *46*, 2329−2339.

(27) Yu, Q.; Lian, J.; Siriponglert, S.; Li, H.; Chen, Y. P.; Pei, S.-S. Graphene Segregated on Ni Surfaces and Transferred to Insulators. *Appl. Phys. Lett.* **2008**, *93*, 113103.

(28) Reina, A.; Thiele, S.; Jia, X.; Bhaviripudi, S.; Dresselhaus, M. S.; Schaefer, J. A.; Kong, J. Growth of Large-area Single- and Bi-layer Graphene by Controlled Carbon Precipitation on Polycrystalline Ni Surfaces. *Nano Res.* **2009**, *2*, 509−516.

(29) Liu, N.; Fu, L.; Dai, B.; Yan, K.; Liu, X.; Zhao, R.; Zhang, Y.; Liu, Z. Universal Segregation Growth Approach to Wafer-Size Graphene from Non-Noble Metals. *Nano Lett.* **2011**, *11*, 297−303.

(30) Weatherup, R. S.; Baehtz, C.; Dlubak, B.; Bayer, B. C.; Kidambi, P. R.; Blume, R.; Schloegl, R.; Hofmann, S. Introducing Carbon Diffusion Barriers for Uniform, High-Quality Graphene Growth from Solid Surfaces. *Nano Lett.* **2013**, *13*, 4624−4631.

(31) Yoon, S.-M.; Choi, W. M.; Baik, H.; Shin, H.-J.; Song, I.; Kwon, M.-S.; Bae, J. J.; Kim, H.; Lee, Y. H.; Choi, J.-Y. Synthesis of Multilayer Graphene Balls by Carbon Segregation from Nickel Nanoparticles. *ACS Nano* **2012**, *6*, 6803−6811.

(32) Bleu, Y.; Barnier, V.; Christien, F.; Bourquard, F.; Loir, A. S.; Garrelie, F.; Donnet, C. Dynamics of Carbon Diffusion and Segregation through a Ni Catalyst, Investigated by XPS during Growth of Nitrogen-Doped Graphene. *Carbon* **2019**, *155*, 410−420.

(33) Lahiri, J.; Miller, T.; Ross, A. J.; Adamska, L.; Oleynik, I. I.; Batzill, M. Graphene Growth and Stability at Ni Surfaces. *New J. Phys.* **2011**, *13*, 025001.
(34) Addou, R.; Dahal, A.; Sutter, P.; Batzill, M. Monolayer Graphene Growth on Ni(111) by Low Temperature Chemical Vapor Deposition. *Appl. Phys. Lett.* **2012**, *100*, 021601.
(35) Lahiri, J.; Miller, T.; Adamska, L.; Oleynik, I. I.; Batzill, M. Graphene Growth on Ni(111) by Transformation of a Surface Carbide. *Nano Lett.* **2011**, *11*, 518−522.
(36) Jacobson, P.; Stöger, B.; Garhofer, A.; Parkinson, G. S.; Schmid, M.; Caudillo, R.; Mittendorfer, F.; Redinger, J.; Diebold, U. Ni Carbide as a Source of Grain Rotation in Epitaxial Graphene. *ACS Nano* **2012**, *6*, 3564−3572.
(37) Josline, M. J.; Kim, E. T.; Lee, J. H. Recent Advances in the Low Temperature Chemical Vapor Deposition Growth of Graphene. *Appl. Sci. Converg. Technol.* **2022**, *31*, 63−70.
(38) Ceyer, S. T.; Gladstone, D. J.; McGonigal, M.; Schulberg, M. T. *Physical Methods of Chemistry*, 2nd ed.; Rossiter, B. W., Baetzold, R. C., Eds.; Wiley: New York, 1993; Vol. *IX-A*, pp 383−452.
(39) Liu, Q. Dynamics of Hydrogen and Low Concentration Carbon on Au-Ni(111) Surface Alloys. Ph.D. Thesis, Massachusetts Institute of Technology, Cambridge, MA, 2018. https://hdl.handle.net/1721.1/118270 (accessed May 4, 2021).
(40) Leon, C. C.; Lee, J.-G.; Ceyer, S. T. Oxygen Adsorption on Au−Ni(111) Surface Alloys. *J. Phys. Chem. C* **2014**, *118*, 29043−29057.
(41) Leon, C. C.; Liu, Q.; Ceyer, S. T. CO Adsorption on Gold Nickel Au−Ni(111) Surface Alloys. *J. Phys. Chem. C* **2019**, *123*, 9041−9058.
(42) Frank, F. C.; van der Merwe, J. H.; Mott, N. F. One-dimensional Dislocations. I. Static Theory. *Proc. R. Soc. London* **1949**, *198*, 205−216.
(43) Jacobsen, J.; Pleth Nielsen, L.; Besenbacher, F.; Stensgaard, I.; Lægsgaard, E.; Rasmussen, T.; Jacobsen, K. W.; Nørskov, J. K. Atomic-Scale Determination of Misfit Dislocation Loops at Metal-Metal Interfaces. *Phys. Rev. Lett.* **1995**, *75*, 489−492.
(44) Nielsen, L. P. The Nucleation and Growth of Au on Ni(110) and Ni(111)−A Scanning Tunneling Microscopy Study. Ph.D. Thesis, Aarhus University, DK-8000 Aarhus C, Denmark, 1995. https://phys.au.dk/fileadmin/site_files/publikationer/phd/Lars_Pleth_Nielsen.pdf (accessed May 4, 2021)
(45) Erley, W.; Ibach, H.; Lehwald, S.; Wagner, H. CO vibrations on a Stepped Ni surface. *Surf. Sci.* **1979**, *83*, 585−598.
(46) Lahr, D. L. Molecular Oxygen Adsorbates at a Au/Ni(111) Surface Alloy and Their Role in Catalytic CO Oxidation at 70−250 K. Ph.D. Thesis, Massachusetts Institute of Technology, Cambridge, MA, 2006. https://dspace.mit.edu/handle/1721.1/36250 (accessed May 4, 2021).
(47) Johnson, A. D.; Maynard, K. J.; Daley, S. P.; Yang, Q. Y.; Ceyer, S. T. Hydrogen Embedded in Ni: Production by Incident Atomic Hydrogen and Detection by High-Resolution Electron Energy Loss. *Phys. Rev. Lett.* **1991**, *67*, 927−930.
(48) Yang, Q. Y.; Maynard, K. J.; Johnson, A. D.; Ceyer, S. T. The Structure and Chemistry of CH_3 and CH Radicals Adsorbed on Ni(111). *J. Chem. Phys.* **1995**, *102*, 7734−7749.
(49) Bürgi, T.; Trautman, T. R.; Haug, K. L.; Utz, A. L.; Ceyer, S. T. Synthesis and Spectroscopic Identification of Ethylidyne Adsorbed on Ni(111). *J. Phys. Chem. B* **1998**, *102*, 4952−4965.
(50) Aizawa, T.; Souda, R.; Ishizawa, Y.; Hirano, H.; Yamada, T.; Tanaka, K.-i.; Oshima, C. Phonon Dispersion in Monolayer Graphite Formed on Ni(111) and Ni(001). *Surf. Sci.* **1990**, *237*, 194−202.
(51) Shikin, A. M.; Farías, D.; Adamchuk, V. K.; Rieder, K. H. Surface Phonon Dispersion of a Graphite Monolayer Adsorbed on Ni(111) and its Modification caused by Intercalation of Yb, La and Cu Layers. *Surf. Sci.* **1999**, *424*, 155−167.
(52) Shikin, A. M.; Prudnikova, G. V.; Adamchuk, V. K.; Moresco, F.; Rieder, K. H. Surface Intercalation of Gold Underneath a Graphite Monolayer on Ni(111) Studied by Angle-resolved Photoemission and High-resolution Electron Energy Loss Spectroscopy. *Phys. Rev. B* **2000**, *62*, 13202−13208.
(53) Al Taleb, A.; Farías, D. Phonon Dynamics of Graphene on Metals. *J. Phys.: Condens. Matter* **2016**, *28*, 103005.
(54) Varykhalov, A.; Sánchez-Barriga, J.; Shikin, A. M.; Biswas, C.; Vescovo, E.; Rybkin, A.; Marchenko, D.; Rader, O. Electronic and Magnetic Properties of Quasifreestanding Graphene on Ni. *Phys. Rev. Lett.* **2008**, *101*, 157601.
(55) GraphPad Prism version 8.0.0 for Windows; GraphPad Software: San Diego, California USA. www.graphpad.com (accessed Sept 7, 2022).
(56) Lehwald, S.; Ibach, H. Decomposition of Hydrocarbons on Flat and Stepped Ni(111) Surfaces. *Surf. Sci.* **1979**, *89*, 425−445.
(57) Jacobsen, K. W.; Nørskov, J. K. Theoretical Study of Carbon Chemisorption on Nickel Surfaces. *Surf. Sci.* **1986**, *166*, 539−553.
(58) Bai, Y.; Kirvassilis, D.; Xu, L.; Mavrikakis, M. Atomic and Molecular Adsorption on Ni(111). *Surf. Sci.* **2019**, *679*, 240−253.
(59) Zhang, W.-X.; Qiao, Q.-A.; Chen, S.-G.; Cai, M.-C.; Wang, Z.-X. Adsorption and Vibration of Carbon on Low Index and Defect Nickel Surface. *Chin. J. Chem.* **2001**, *19*, 325−331.
(60) Ricca, A.; Bauschlicher, C. W., Jr.; Boersma, C.; Tielens, A. G. G. M.; Allamandola, L. J. The Infrared Spectroscopy of Compact Polycyclic Aromatic Hydrocarbons Containing up to 384 Carbons. *Astrophys. J.* **2012**, *754*, 75.
(61) Wiltner, A.; Linsmeier, Ch.; Jacob, T. Carbon Reaction and Diffusion on Ni(111), Ni(100), and Fe(110): Kinetic Parameters from X-ray Photoelectron Spectroscopy and Density Functional Theory Analysis. *J. Chem. Phys.* **2008**, *129*, 084704−084711.
(62) High, E. A. Surface Effects in State-Resolved Gas-Surface Reaction. Ph.D. Thesis, Tufts University, Medford, MA, 2020.
(63) Seah, M. P.; Dench, W. A. Quantitative Electron Spectroscopy of Surfaces: A Standard Data Base for Electron Inelastic Mean Free Paths in Solids. *Surf. Interface Anal.* **1979**, *1*, 2−11.
(64) Ceyer, S. T. The Unique Chemistry of Hydrogen Beneath the Surface: Catalytic Hydrogenation of Hydrocarbons. *Acc. Chem. Res.* **2001**, *34*, 737−744.
(65) Hammer, B.; Nørskov, J. K. Theoretical Surface Science and Catalysis − Calculations and Concepts. In *Advances in Catalysis*; Gates, B. C., Knozinger, H., Eds.; Academic Press: San Diego, CA, 2000; Vol. *45*, pp 71−129.
(66) Kitchin, J. R.; Nørskov, J. K.; Barteau, M. A.; Chen, J. G. Role of Strain and Ligand Effects in the Modification of the Electronic and Chemical Properties of Bimetallic Surfaces. *Phys. Rev. Lett.* **2004**, *93*, 156801.
(67) Hammer, B.; Nørskov, J. K. Electronic Factors Determining the Reactivity of Metal Surfaces. *Surf. Sci.* **1995**, *343*, 211−220.
(68) Nørskov, J. K.; Abild-Pedersen, F.; Studt, F.; Bligaard, T. Density Functional Theory in Surface Chemistry and Catalysis. *Proc. Natl. Acad. Sci. U.S.A.* **2011**, *108*, 937−943.
(69) Besenbacher, F. I.; Chorkendorff, B. S.; Clausen, B.; Hammer, A. M.; Molenbroek, J. K.; Nørskov, I.; Stensgaard, I. Design of a Surface Alloy Catalyst for Steam Reforming. *Science* **1998**, *279*, 1913−1915.
(70) Abild-Pedersen, F.; Nørskov, J. K.; Rostrup-Nielsen, J. R.; Sehested, J.; Helveg, S. Mechanisms for Catalytic Carbon Nanofiber Growth Studied by Ab Initio Density Functional Theory. *Phys. Rev. B* **2006**, *73*, 115419.
(71) Jiao, M.; Qian, H.; Page, A.; Li, K.; Wang, Y.; Wu, Z.; Irle, S.; Morokuma, K. Graphene Nucleation from Amorphous Ni Carbides: QM/MD Studies on the Role of Subsurface Carbon Density. *J. Phys. Chem. C* **2014**, *118*, 11078−11084.
(72) Arifin, R.; Shibuta, Y.; Shimamura, K.; Shimojo, F. First Principles Molecular Dynamics Simulation of Graphene Growth on Ni(111). *Mater. Sci. Eng.* **2016**, *128*, 012032.
(73) Zhan, H.; Jiang, B.; Zietz, O.; Olsen, S.; Jiao, J. Simulation to Fabrication-Understanding the Effect of NiAuCu Alloy Catalysts for Controlled Growth of Graphene at Reduced Temperatures. *Mater. Res. Express* **2020**, *7*, 015603.

https://doi.org/10.1021/jacs.2c13205
J. Am. Chem. Soc. 2023, 145, 6299−6309

(74) Weatherup, R. S.; Bayer, B. C.; Blume, R.; Ducati, C.; Baehtz, C.; Schlögl, R.; Hofmann, S. In Situ Characterization of Alloy Catalysts for Low-Temperature Graphene Growth. *Nano Lett.* **2011**, *11*, 4154−4160.
(75) Olson, S.; Zietz, O.; Tracy, J.; Li, Y.; Tao, C.; Jiao, J. Low Temperature Chemical Vapor Deposition Growth of Graphene Films Enabled by Ultrathin Alloy Catalysts. *J. Vac. Sci. Technol. B* **2020**, *38*, 032202.
(76) Feng, Y.; Yao, X.; Hu, Z.; Xu, J. J.; Zhang, L. Passivating a Transition Metal Surface for More Uniform Growth of Graphene: Effect of Au Alloying on Ni(111). *Phys. Rev. B* **2013**, *87*, 195421.
(77) Bengaard, H. S.; Nørskov, J. K.; Sehested, J.; Clausen, B. S.; Nielsen, L. P.; Molenbroek, A. M.; Rostrup-Nielsen, J. R. Steam Reforming and Graphite Formation on Ni Catalysts. *J. Catal.* **2002**, *209*, 365−384.
(78) Huang, Y.; Du, J.; Zhou, T.; Ling, C.; Wang, S.; Geng, B. Role of Au in Graphene Growth on a Ni Surface. *ACS Catal.* **2014**, *4*, 892−902.

Recommended by ACS

Role of Kinetics and Thermodynamics in Controlling the Crystal Structure of Nickel Nanoparticles Formed on Reduced Graphene Oxide: Implications for Energy Storag...

Mahmound Tamadoni Saray, Reza Shahbazian-Yassar, *et al.*
JUNE 09, 2023
ACS APPLIED NANO MATERIALS
READ

Formation of Large-Area Twisted Bilayer Graphene on Ni(111) Film via Ambient Pressure Chemical Vapor Deposition

Weicheng Qiu, Mengchun Pan, *et al.*
MARCH 08, 2023
ACS APPLIED ELECTRONIC MATERIALS
READ

Molecular Bridge Engineering for Tuning Quantum Electronic Transport and Anisotropy in Nanoporous Graphene

César Moreno, Aitor Mugarza, *et al.*
MARCH 29, 2023
JOURNAL OF THE AMERICAN CHEMICAL SOCIETY
READ

Electrical Control of Chemical Vapor Deposition of Graphene

Jiangtao Wang, Jing Kong, *et al.*
DECEMBER 07, 2022
JOURNAL OF THE AMERICAN CHEMICAL SOCIETY
READ

Get More Suggestions >

https://doi.org/10.1021/jacs.2c13205
J. Am. Chem. Soc. 2023, 145, 6299−6309